RSC Advances

PAPER

View Article Online
View Journal | View Issue

Cite this: *RSC Adv.*, 2022, **12**, 28414

Preparation and electrical properties of inorganic electride $[Y_2Ti_2O_6]^{2+}(2e^-)$

Yong Liu,[abc] Hengwei Wei,[b] Xiaoming Wang,[b] Huan Jiao *[b] and Xiping Jing*[c]

Oxygen-depleted samples $[Y_2Ti_2O_{7-x}]^{2x+}(2xe^-)$ ($0 \le x \le 1.0$) were prepared by reducing Y_2TiO_7 powders at 500 °C to 650 °C using CaH_2 as a reductive agent, where x represents the content of $V_O(V_O^{\times} + V_O^{\cdot})$, which was determined by thermogravimetric analysis. Powder X-ray diffraction patterns illustrate that the pure pyrochlore phase is kept for the samples with $x \le 1.0$, whereas the apparent x values surpass 1.0, and the impurity phase Y_2O_3 appears. The electride $[Y_2Ti_2O_{7-x}]^{2x+}(2xe^-)$ ($x \approx 1.0$) can be obtained under a reductive condition, in which the concentration of V_O is 7.75×10^{21} cm^{-3}. The electron paramagnetic resonance measurements gave the concentration of unpaired electrons in the electride as 1.30×10^{21} cm^{-3}, indicating that the degree of the ionization of $V_O^{\times}$ is less than 10%. Conductivity measurements for a sintered pellet sample (relative density ~ 70%) indicate that the electride has quite high conductivity (~1.09 S cm^{-1} at 300 K). The conduction was interpreted by using the variable range hopping mechanisms.

Received 16th September 2022
Accepted 21st September 2022

DOI: 10.1039/d2ra05847b

rsc.li/rsc-advances

Introduction

Electrides are a kind of material in which electrons serve as anions.[1] It was found that electrides were formed when the alkali metal and alkali earth metals were dissolved into liquid ammonia at low temperatures. As an example, when the metal Na is dissolved into liquid ammonia, the Na atoms are ionized and form solvated Na^+ [$Na(am)_n^+$, am = ammonia] as cations. At the same time, the generated electrons are also solvated [$e(am)_m^-$], which play the role of anions. The reactions between alkali metals and crown ethers also lead to the formation of electrides. In the crystal of $Cs(18crown\text{-}6)_2$ complex, Cs^+ is coordinated by two 18crown-6, forming $[Cs(18crown\text{-}6)_2]^+$ as cations, while the "electron-anions" generated from the ionization of the Cs atoms take the interstitial positions constructed by the $[Cs(18crown\text{-}6)_2]^+$ cations. Due to the existence of the solvated electrons, the electrides are very strongly reductive agents.[1] However, these electrides are only stable at low temperatures and very sensitive to air and moisture. Thus, their applications are impeded.

Recently, Matsushi *et al.* reported an inorganic solid electride–fully reduced mayenite $[Ca_{12}Al_{14}O_{32}]^{2+}(2e^-)$,[2] which is stable at ambient temperature and atmosphere. The original composition of mayenite can be represented as $Ca_{12}Al_{14}O_{33}$, which is a neutral material. This material has a tetragonal unit cell, containing two molecules ($Ca_{12}Al_{14}O_{33} \times 2$). The lattice framework is constructed by $[Ca_{12}Al_{14}O_{33} \times 2]^{4+}$ with the positive charge composing 12 cages, 2 relatively loosely bonded O^{2-} take the positions in 2 out of 12 cages.[2,3] When the material is thermally treated in a reductive atmosphere, part of the loosely bonded O^{2-} ions may escape as O_2 from the lattice and leave electrons in the cages, considered as the electron captured oxygen vacancy $V_O^{\times}$, or *F*-center. With the proper reductive condition, all of the loosely bonded O^{2-} ions can be removed from the lattice. In this case, the relatively free electrons captured at $V_O^{\times}$ play the role of anions. Thus the material is considered as the electride. The concentration of the "free electrons" is high in the lattice. Therefore, the electride has high conductivity. Since some of the "free electrons" are unpaired, the magnetic properties are also attractive. The inorganic electrides would be potentially used as reductive agents, electron-emitters, *etc*[2,4]. Additionally, it was also reported[5,6] that these materials were applied as catalysts for the NH_3 synthesis and CO oxidation. The finding of the inorganic solid electride $[Ca_{12}Al_{14}O_{32}]^{2+}(2e^-)$ stimulates the research interest in exploring more inorganic solid electrides.

In this work, we choose $Y_2Ti_2O_7$ with the pyrochlore structure as a starting material to prepare electrides. As we know, Ti^{4+} ions in titanates have the potential to be reduced into Ti^{3+} when they are treated at high temperatures or in reductive atmospheres. At the same time, some O^{2+} ions may escape from the lattice as O_2, leaving the oxygen vacancies V_O (including $V_O^{\times}$ and $V_O^{\cdot}$) in the lattice.[7,8] The materials containing V_O with relatively high concentrations are named oxygen-depleted (simplified as O-depleted) materials. The composition of the O-depleted $Y_2Ti_2O_7$ can be represented as $Y_2Ti_2O_{7-x}$. Additionally, the pyrochlore structure, $Y_2Ti_2O_7$ has one oxygen not bonded to Ti

[a]*The Guyuan Museum of Ningxia, Guyuan 756000, P. R. China*
[b]*Key Laboratory of Macromolecular Science of Shaanxi Province, College of Chemistry and Chemical Engineering, Shaanxi Normal University, Xi'an 710062, P. R. China. E-mail: jiaohuan@snnu.edu.cn*
[c]*The State Key Laboratory of Rare Earth Materials Chemistry and Applications, College of Chemistry and Molecular Engineering, Peking University, Beijing 100871, P. R. China. E-mail: xpjing@pku.edu.cn*

atoms. Thus it might be possible to prepare the O-depleted $Y_2Ti_2O_7$ with a high concentration of V_O, or even let the x value approach 1.0, with which the material would be considered as an electride.

Actually, the research to prepare the O-depleted pyrochlore could be found in the 1960s. In Goodenough's work,[9] the Pb-noble metal pyrochlores ($Pb_2M_2O_{7-x}$, M = Ru, Ir, Re) with O-depletion were prepared, and the materials with $x = 1.0$ were obtained. However, in this work, the concept of electride was not mentioned, and the functional properties (*i.e.* conductive or magnetic properties) were not studied. The research for the O-depleted $Y_2Ti_2O_7$ ($Y_2Ti_2O_{7-x}$) appeared in this century,[10,11] in which the materials with $x \approx 1.0$ were prepared, and the conductivities and magnetic susceptibilities were measured. It is a pity that the concept of the electride was not applied to interpret the work either. Therefore, further research on the O-depleted $Y_2Ti_2O_7$ is imperative.

In this work, the reductive conditions were explored for preparing the O-depleted $Y_2Ti_2O_7$, and the electride with the composition $Y_2Ti_2O_6$ ($x \approx 1.0$) was obtained, which would be represented as $[Y_2Ti_2O_6]^{2+}(2e^-)$. The contents of V_O and the concentration of unpaired electrons in the lattice were measured. The conductive properties of the electride $Y_2Ti_2O_6$ were characterized.

2 Experimental

Powder samples of the starting material $Y_2Ti_2O_7$ were synthesized by solid-state reactions from stoichiometric mixtures of the raw materials TiO_2 (A. R.) and Y_2O_3 (99.99%) at 1400 °C for 13 h in air. Prior to heating, the raw materials were thoroughly mixed by grindings in an agate mortar with a pestle. As-prepared powder samples of $Y_2Ti_2O_7$ have a white (or pale) body color.

The powder samples of the O-depleted $Y_2Ti_2O_7$ were prepared from the powder of $Y_2Ti_2O_7$ by using the solid reducing approach, in which the solid reductive agent CaH_2 was applied. The powder mixtures of $Y_2Ti_2O_7$ (~0.5 g) and CaH_2 in various mass ratios were ground in a glovebox (Mikrouns, Ar atmosphere, O_2 < 1 ppm, H_2O < 1 ppm), and then sealed in vacuumed quartz ampoules (~5 ml). The sealed samples were heated at various temperatures ranging from 500–650 °C with various time 5–40 h. After heating, crash the quartz ampoules and take the samples out. The samples were washed using deionized water for several times until the supernatant approached to neutral in order to remove Ca^{2+} and OH^- ions. Finally, the washed samples were dried at 140 °C for 2 h in an oven. The reduced treatments lead to the samples becoming dark.

For conductivity measurements, the pellets of the O-depleted samples were sintered. The powder samples were mixed with a few drops of 5% polyvinyl alcohol solution as a binder and then were pressed into pellets with 10 MPa pressure in stainless steel die. The pellets were sealed in the vacuumed quartz ampoules and sintered at 950 °C for a short time ~2 h, in order to avoid a large change in the sample status. The obtained pellets had the dimension ~1.0 cm in diameter and ~0.15 cm in thickness with a relative density of ~70%.

The phase purity of samples was characterized by X-ray diffraction (XRD) using a Rigaku Dmax2000 X-ray powder diffractometer (Japan) with Cu Kα radiation ($\lambda = 0.15418$ nm) at 40 kV and 100 mA. The XRD patterns were collected in the 2θ range 10° ~ 80° with the scanning rate of 8° min^{-1}. Electron paramagnetic resonance (EPR) measurements were performed at ~9.4 GHz (X-band) using a Bruker A300 10-12 EPR spectrometer (Germany). The concentrations of unpaired electrons in the samples were determined by using the method supplied in ref. 12, in which the areas of the microwave absorption bands were calculated by twice integrations of the original EPR spectra ("dA/dH–H" plots, A is the microwave absorption of the samples and H is the strength of the magnetic field), and $CuSO_4 \cdot 5H_2O$, diluted by Al_2O_3 powders with the mass ratio $CuSO_4 \cdot 5H_2O : Al_2O_3 = 1 : 9$, was applied as a standard. Both the XRD and EPR measurements were carried out at room temperature. Thermal analyses were conducted on a simultaneous differential scanning calorimeter–thermogravimetric analyzer (DSC-TGA, Q600STD, Thermal Analysis, USA). The data were collected from room temperature to 1200 °C with the temperature increasing rate of 20 °C min^{-1} and air as flowing gas.

The conductivities of the sintered pellets were measured in the temperature range 80–450 K using a four-wire setup, and Pt wires were cemented by Ag paste on the two opposite surfaces of the pellet samples. The temperature environment was provided by a closed cycle refrigerator (Janis VPF-100, UAS) using the liquid N_2 as the refrigerant. The temperature was regulated by a M331 temperature controller (LakeShore, USA). A SB118 current source and a PZ158A voltmeter (Shanghai Qianfeng Electronic Instruments, China) were used for data collection.

3 Results and discussion

3.1 Description of the $Y_2Ti_2O_7$ structure

$Y_2Ti_2O_7$ takes a pyrochlore structure with the face-center cubic unit ($a = 1.00979$ nm) and the space group $Fd3m$ (no. 227), which contains 8 $Y_2Ti_2O_7$.[13] The structure is constructed by Ti–O framework and O–Y framework. In the Ti–O framework, the $[Ti_4O_{18}]^{20-}$ cluster is the framework unit, in which each TiO_6 octahedron shares its three corners with other 3 TiO_6 octahedrons [Fig. 1(a)]. Each $[Ti_4O_{18}]^{20-}$ cluster shares its 12 outer

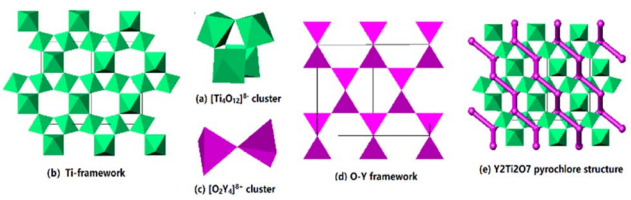

Fig. 1 Pyrochlore structure of $Y_2Ti_2O_7$: (a) $[Ti_4O_{12}]^{8-}$ cluster–the unit of the Ti–O framework; (b) Ti–O framework; (c) $[O_2Y_4]^{8+}$ cluster–the unit of the O–Y framework; (d) O–Y framework; (e) the $Y_2Ti_2O_7$ structure – the Ti–O and O–Y frameworks interpenetrate each other. The $[O_2Y_4]^{8+}$ clusters are simplified as sticks.

corners with the other 8 $[Ti_4O_{18}]^{20-}$ clusters, extending to 3-dimensional framework. The average composition of the Ti–O framework is $[Ti_4O_{12}]$. The $[Ti_4O_{12}]$ framework has 3-member rings, denoted as [T], and 6-member rings, denoted as [H] viewing along [110] direction. The number ratio [T] : [H] is 2 : 1 [Fig. 1(b)]. In the O–Y framework, 2 OY_4 tetrahedrons connecting each other by sharing one corner construct the $[O_2Y_7]^{17+}$ cluster as the framework unit [Fig. 1(c)]. Each $[O_2Y_7]^{17+}$ cluster contributes its six outer corners to link other 6 $[O_2Y_4]^{8+}$ clusters, forming 3D framework [Fig. 1(d)]. The average composition of the O–Y network is $[O_2Y_4]^{8+}$. The Ti–O framework and the O–Y framework interpenetrate each other, building the 3-dimensional pyrochlore structure, in which the O–Y framework extends through the [H] rings of the Ti–O framework and the [T] rings are left empty [Fig. 1(e)]. The structure data indicated in the formula $Y_2Ti_2O_7$, 6 O link to Ti, constructing the TiO_6 octahedron and 1 O links to Y, taking the site at the center of the OY_4 tetrahedron. In the 1970s, some authors[14–16] calculated the electrostatic energies of the $[Ti_4O_{12}]$ and $[O_2Y_4]$ frameworks, indicating that the former is much higher than the later. Therefore, it might be deduced that the oxygen atoms in the OY_4 tetrahedrons are easier to be removed out from the lattice than the oxygen atoms in the TiO_6 octahedrons. If $Y_2Ti_2O_7$ is thermally treated in a reductive atmosphere, and the oxygen vacancies V_O tend to take the sites at the centers in the OY_4 tetrahedrons.

3.2 Investigation of the reductive conditions

The starting material $Y_2Ti_2O_7$ was prepared by the routine solid state reactions, which was described in the "experimental" section. The XRD pattern of the as-prepared sample shown in Fig. 2 illustrates that the pattern matches well to the related JCPDS file 42-413. Thus, the as-prepared $Y_2Ti_2O_7$ is a pure phase sample. In order to change the starting material to the O-depleted material or the electride, thermally reducing treatments are necessary for $Y_2Ti_2O_7$. The reducing process was also described in the "experimental" section. For obtaining high content of V_O, the reductive conditions should be chosen as strong as possible, but the phase purity should be kept.

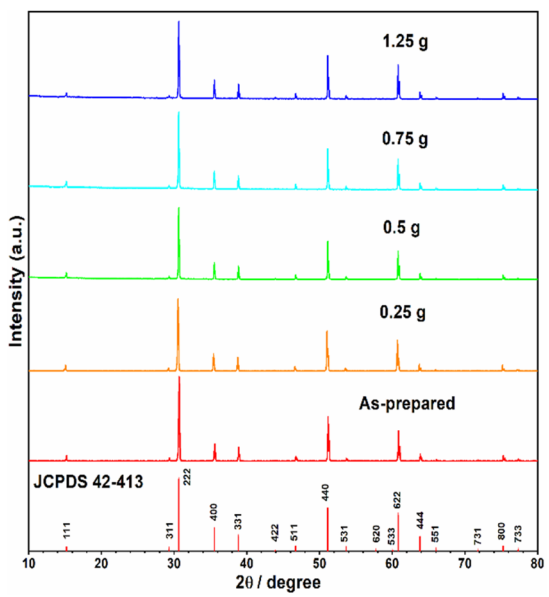

Fig. 2 XRD patterns of JCPDS file (42-413), the as-prepared samples as well as the samples (0.5 g) mixed with various weights of CaH_2 annealed at 500 °C for 16 h in vacuumed quartz ampoules.

Firstly, the influence of the mass of CaH_2 to the phase purity was investigated. The $Y_2Ti_2O_7$ powder samples (0.5 g for each) were mixed with various amounts of CaH_2 (0.25 g–1.25 g), and annealed at 500 °C for 16 h. After the reducing treatment, the white powders of $Y_2Ti_2O_7$ became dark, which can be explained by the defect reactions and chemical reactions. When $Y_2Ti_2O_7$ is annealed at a high temperature (*e.g.* above 500 °C), the defect reaction (1) occurs, and the oxygen vacancies $V_O^{\times}$ are produced:

$$O_O^{\times} \leftrightarrow V_O^{\times} + (1/2)O_2\uparrow \quad (1)$$

In the ambient atmosphere, eqn (1) only shifts to right slightly, and the $V_O^{\times}$ content is not very high. In this research, the solid reductive agent CaH_2 was added, thus the below chemical reaction was involved in the process and O_2 produced in eqn (1) was reduced by CaH_2:

$$O_2 + CaH_2 \rightarrow Ca(OH)_2 \quad (2)$$

Thus the addition of CaH_2 lead to right-shift of eqn (1) in a large extent and the $V_O^{\times}$ content increased significantly. In this research, it is respected that 1 mole O atoms should be removed, and 1 mole $V_O^{\times}$ should be produced. In addition, $V_O^{\times}$ may be ionized and transfer an electron to $Ti_{Ti}^{\times}$:

$$V_O^{\times} \leftrightarrow V_O^{\cdot} + e' \quad (3)$$

$$Ti_{Ti}^{\times} + e' \leftrightarrow Ti'_{Ti} \quad (4)$$

or

$$V_O^{\times} + Ti_{Ti}^{\times} \leftrightarrow V_O^{\cdot} + Ti'_{Ti} \quad (5)$$

For brief discussion, the second step of the ionization $V_O^{\cdot} \rightarrow V_O^{\cdot\cdot}$ is omitted. Since all three kinds of defects $V_O^{\times}$, $V_O^{\cdot}$ and Ti'_{Ti} have loosely bound electrons, the levels of which may be located in the band gap below the conduction band. These loosely bound electrons may be excited to the conduction band by the visible light, resulting in the dark body color of the reduced samples.

The XRD patterns of the samples thermally treated with various amounts of CaH_2 are shown in Fig. 2. The patterns of all the samples are in good agreement with that of JCPDS file 42-413 and no clear peaks related to any impurity phases were observed, thus, all the reduced samples are phase pure, which indicated that the mass of CaH_2 was not very sensitive to the phase purity of the reduced samples and the CaH_2 weights used in this work were all suitable. However, in order to keep a relatively strong reductive conditions, the CaH_2 weight of 0.75 g was chosen for the further work.

Then optimized reducing temperature was investigated. Several powder samples of $Y_2Ti_2O_7$ (0.5 g for each) mixed with 0.75 g CaH_2 were annealed at various temperatures (500 °C–650 °C). The XRD patterns represented in Fig. 3 indicate that if the reducing temperature is below 600 °C, the reduced samples are phase pure; whereas if it is above 650 °C, impurity phase of Y_2O_3 appears. The suitable temperature was decided as 600 °C for the reducing annealing.

Furthermore, the influence of annealing time to the phase purity was explored. The powder samples of $Y_2Ti_2O_7$ (0.5 g for each) mixed with 0.75 g CaH_2 were annealed at 600 °C for various time (5–40 h). The XRD patterns (in Fig. 4) clearly shows that the reducing time 20 h may be considered as an optimized time. If the reducing time surpasses 20 h, the peaks of the impurity phase Y_2O_3 appear.

In summary, to prepare electrides or O-depleted samples, the suitable reductive conditions are decided: the starting material $Y_2Ti_2O_7$ 0.5 g mixed with the reductive agent CaH_2 0.75 g is annealed at 600 °C for 20 h.

3.3 Measurements of the content of the oxygen vacancies V_O

In 3.2 section, it was deduced that after reducing treatment, the oxygen vacancies V_O (including $V_O^{\times}$ and $V_O^{\cdot}$) may be formed. In this section, the existence of V_O would be proved by TG measurements.

The TG measurements (Fig. 5) were conducted for the samples previously annealed with 0.75 g CaH_2 at 600 °C for various time, 5–40 h. The TG data indicate that with the increase of the temperature from ~320–~620 °C, the weights of the samples enhance clearly and the weight increments are about several percent. The samples previously annealed longer time in the reductive conditions have larger increments.

In 3.2 section, it was deduced that after reduction by CaH_2, the samples have quit high contents of V_O. In this case, the composition of the material can be represented by the formula $Y_2Ti_2O_{7-x}$. The x represents the content of V_O in the lattice. The reaction that occurred during TG measurements can be represented as:

$$Y_2Ti_2O_{7-x} + (x/2)\ O_2 \rightarrow Y_2Ti_2O_7 \quad (6)$$

Eqn (6) means that during TG measurements, the $V_O^{\cdot\cdot}$ contained samples are oxidized by O_2 and the O atoms enter the lattice filling the oxygen vacancies V_O, leading to the weight increments, *i.e.* Eqn (1) shifts to left. The larger the x value, the

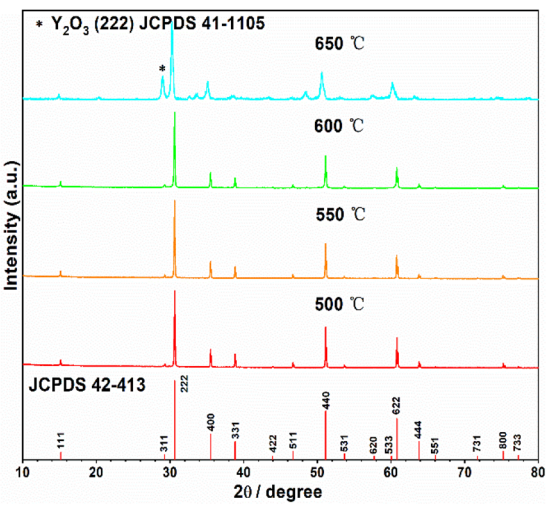

Fig. 3 XRD patterns of the samples (0.5 g) mixed with 0.75 g CaH_2 annealed at various temperatures for 16 h in vacuumed quartz ampoules. For comparison, the pattern of JCPDS file (42-413) is represented.

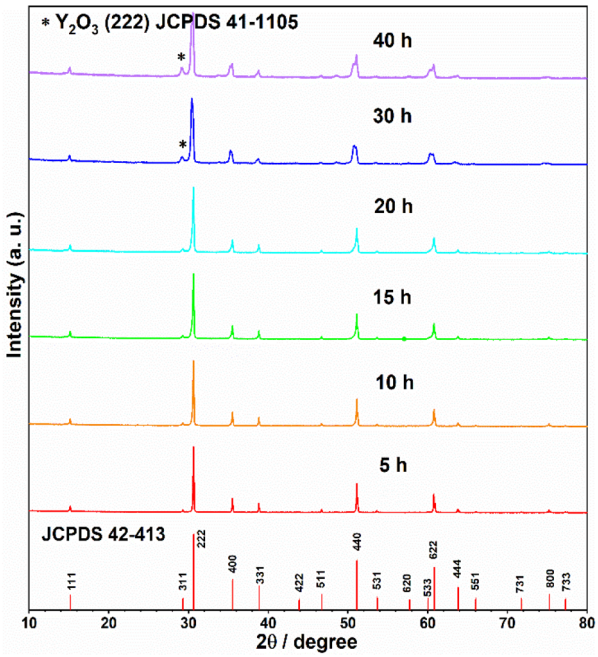

Fig. 4 XRD patterns of the samples (0.5 g) mixed with 0.75 g CaH_2 annealed at 600 °C for the various time in vacuumed quartz ampoules. For comparison, the pattern of JCPDS file (42-413) is represented.

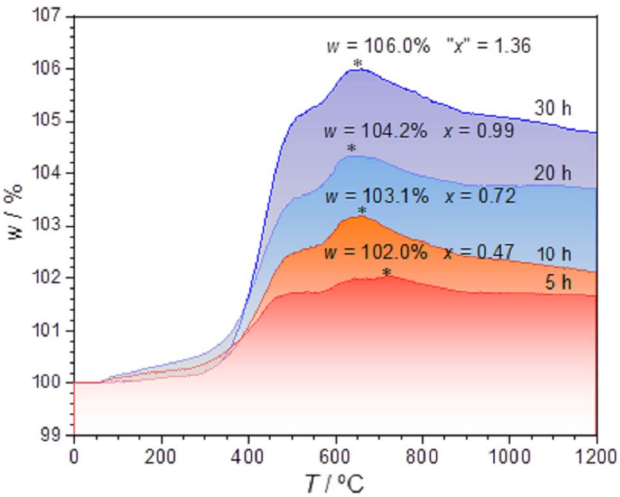

Fig. 5 TG curves of the samples previously annealed with 0.75 g CaH_2 at 600 °C for various time.

larger the weight increment is. According to the values of the weight increments, the x values (the V_O contents) can be calculated, showed in Fig. 5. For the sample previously annealed with CaH_2 for 5 h, the V_O content x is 0.47. With an increase of the annealing time, the x value increases. When the annealing time increases to 20 h, the x value approaches 1.0, which illustrates that one mole of oxygen atoms are removed out from the lattice, and one mole V_O is formed. As we know, $V_O^\times$ has two loosely bound electrons (maybe, some of them are ionized and transferred to the Ti'_{Ti} sites, but the total number of the loosely bound electrons are not changed), which may play the role of the anions. Thus this sample is considered as an electride, the composition of which can be represented as $[Y_2Ti_2O_6]^{2+}(2e^-)$. For the sample with annealing time 30 h, the apparent "x" value is 1.36 (over 1.0). However, the XRD data (Fig. 4) indicate that this sample is over reduced and is not phase pure, thus this "x" value is insignificance. The TG curves also show that the samples have slight weight loss above 620 °C. It is mostly possible that eqn (1) slightly shifts to right at higher temperatures since it is an entropy increasing reaction (solid O becomes gaseous O).

There is another possibility that the reducing treatments does not produce V_O, but the loss of oxygen leads to the reduction of Ti^{4+} to Ti^{3+}. If this is the case, for the sample $x = 1$, 1 O was lost, which would result in 2 Ti^{4+} were reduced to Ti^{3+}. In other words, in this sample, all Ti were reduced from Ti^{4+} to Ti^{3+}. XRD pattern (Fig. 4) revealed this sample has pure phase of pyrochlore. It could not be imaged that Ti^{3+} compound could have the same structure as Ti^{4+} compound. Therefore, it is believed that the reducing treatments produce $V_O^\times$ in the lattice, rather than reduce Ti^{4+} to Ti^{3+}. It is known that the ionization of $V_O^\times$ may produce Ti^{3+}, described in eqn (4) or (5), but only small amount of Ti^{4+} can be reduced (see 3.4 section), thus the pyrochlore structure can be kept. Actually, ref. 10 and 11 support the formation of V_O in the lattice after reducing treatments.

In 3.1 section, it was described that the $Y_2Ti_2O_7$ structure was constructed by two frameworks of $[Ti_4O_{12}]$ and $[O_2Y_4]$ interpenetrated each other. Theoretic calculations[14–16] indicated that the electrostatic energy of the $[Ti_4O_{12}]^{8-}$ cluster was much larger than that of $[O_2Y_4]^{8+}$. Thus, it is deduced that the oxygen vacancies V_O tend to be formed by removing the oxygen atoms out from the center of the OY_4 tetrahedrons. Goff, *et al.*[10] conducted the structure refinement of the O-depleted $Y_2Ti_2O_{6.79}$ based on the neutron diffraction data. The site occupancies also indicated that the oxygen vacancies V_O are prefer to stay at the centers of the OY_4 tetrahedrons. As we know, in $Y_2Ti_2O_7$, 6 O link Ti and only 1 O links Y. For the sample with the value $x \approx 1.0$, all the oxygens at the centers of the OY_4 tetrahedrons were removed out.

3.4 Measurements of the concentration of the unpaired electrons

In 3.2 section, it was presumed that once the oxygen vacancies $V_O^\times$ were formed in the lattice, they would be ionized and transfer electrons to Ti, represented by eqn (3) and (4). In this case, two kinds of defects $V_O^\cdot$ and Ti'_{Ti} would exist, each of which has one unpaired electron. These defects can be characterized by using EPR.

A selected EPR spectrum for the sample annealed with 0.75 g CaH_2 at 600 °C for 20 h is illustrated Fig. 6. The composition of the sample in Fig. 6 can be represented as $Y_2Ti_2O_{7-x}$ ($x \approx 1.0$). This formula indicates that the sample has 1 mole of V_O in the lattice, which is a quite high concentration of the defect. The high concentration of V_O leads to lattice distortion, further it causes the broadening, deformation and overlapping of the EPR peaks, thus it is not easy to give clear assignments for this spectrum. Here, we would like to consider the peaks P_1 to P_3. Refer to the assignments given in ref. 17–20 for some titania and titanates, the peak with $g < 2.0$ (P_2) is assigned to $V_O^\cdot$; the peak with $g < 2.0$ (P_1) is assigned to Ti^{3+} (Ti'_{Ti}). In fact, besides the electron transferring processes described in eqn (3)–(5), in the lattice, there are other electron transferring processes, *e.g.* the electrons transfer to the O_2 absorbed on the surface:

$$V_O^\times + O_2 \leftrightarrow V_O^\cdot + O_2^- \quad (7)$$

P_3 has a g value larger than 2.0, which may be assigned to O_2^-. Actually, there are some peaks with poor resolution at lower magnetic fields, which might be related to some unknown defects containing unpair electrons, but they could not be assigned at this stage. The assignments for the above EPR peaks support the discussions in 3.2 and 3.2 sections about the formation of V_O as well as the electron transfer processes, thus they also support that the sample related to Fig. 6 ($Y_2Ti_2O_{7-x}$, $x \approx 1.0$) is an electride.

A series EPR spectra were collected for the samples annealed with 0.75 g CaH_2 at 600 °C for various times, *i. e.* for the samples $Y_2Ti_2O_{7-x}$ with various values of x, represented in Fig. 7(a). The spectra in Fig. 7(a) have a similar profile to that in Fig. 6, which means these samples have the defects $V_O^\cdot$, Ti'_{Ti} and O_{2-}. By using these EPR data, the concentrations of the unpaired electrons varied with annealing time (or x) can be calculated. The calculation equation was recommended by Weil, *et al.*[12] In these calculations, $CuSO_4 \cdot 5H_2O$ powder (mixed with Al_2O_3 in the mass ratio $W_{CuSO_4 \cdot H_2O} : W_{Al_2O_3} = 1 : 9$) was used as the standard.

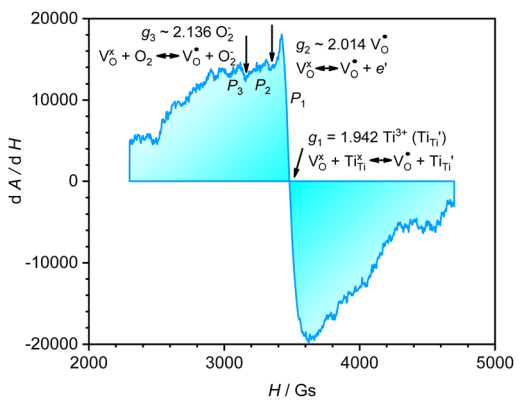

Fig. 6 EPR spectrum of the sample annealed with 0.75 g CaH_2 at 600 °C for 20 hours.

The EPR spectra for both the samples and the standard were collected in the same measuring conditions so as the parameters related to the instrument set-up, the signal amplification, and the scanning scale in the equation can be reduced. On the other hand, all of the defects $V_O^{\cdot}$ and Ti'_{Ti}, as well as Cu^{2+} in the standard are the one-unpaired-electron centers and they all have the total spin quantum number $S = 1/2$, thus the quantum number S also can be eliminated from the equation. The simplified equation for calculating the concentration of the unpaired electrons $[e]$ can be represented as:

$$[e] = \frac{A_s (g_{CuSO_4})^2}{A_{CuSO_4} (g_s)^2} \times \frac{m_{CuSO_4} \times N_A}{FW_{CuSO_4}} \times \frac{D_s}{m_s} \quad (8)$$

Here N_A is Avogadro's number; the subscript letter s denotes the samples and $CuSO_4$ denotes the standard $CuSO_4 \cdot 5H_2O$; The parameter A is the area of the EPR absorption band. By integrating the original EPR spectra, which are in differential form (dA/dH–H), the absorption bands are obtained [Fig. 7(b)]. The A values can be calculated by the second integration of the EPR spectra. g is the electron spin g factor, which can be calculated based on the EPR spectra. In this work, g_{CuSO4} was measured as 2.192 and the values of g_s vary from 1.925 to 1.960, which is labelled for each spectrum in Fig. 7(a) m, FW and D represent the mass, formula weight and density, respectively. Since the resolutions of the spectra are poor, we could not calculate the concentration for each defect, but we may calculate the total concentration of the unpaired electrons approximately.

The calculation results are illustrated in the inset in Fig. 7(b). For the sample annealed with CaH_2 for five h ($x = 0.47$), the concentration of the unpaired electrons $[e]$ is about 3.93×10^{20} cm^{-3}. When the annealing time increases, the $[e]$ value increases and it approaches a maximum of $\sim 1.30 \times 10^{21}$ cm^{-3} for the sample with an annealing time of 20 h ($x \approx 1.0$). Further increasing the annealing time, $[e]$ decreases gradually since they were over-reduced and impurity phase appeared.

For the sample with an annealing time of 20 h, the V_O content x is about 1.0 (refer to the formula $Y_2Ti_2O_{7-x}$), which corresponds to the concentration of V_O (it includes both $V_O^{\times}$ and $V_O^{\cdot}$) as 7.75×10^{21} cm^{-3}. However, $[e]$ is about 1.30×10^{21} cm^{-3}, much less than $[V_O]$, probably due to incomplete ionization. According to eqn (3)–(5) and (7), $[e]$ is the sum of the concentrations of $V_O^{\cdot}$, Ti'_{Ti}, O_{2-} as well as some unknown defects containing unpaired electrons. Except for $V_O^{\cdot}$, all the unpaired electrons on the various defects come from the ionization of $V_O^{\times}$, thus $[V_O^{\cdot}] = [e]/2$. Further, the degree of ionization (α) of $V_O^{\times}$ can be calculated as

$$\alpha = \frac{[V_O^{\cdot}]}{[V_O^{\times}] + [V_O^{\cdot}]} = \frac{[e]/2}{V_o} = 8.4\% \quad (9)$$

Only less than 10% of $V_O^{\times}$ is ionized. Although the concentration of V_O is quite high, the concentrations of $V_O^{\cdot}$ and Ti'_{Ti} are not high. Most V_O takes the form of $V_O^{\times}$, *i.e.,* most loosely bound electrons are trapped at $V_O^{\times}$. Therefore, it is reasonable to consider the sample $Y_2Ti_2O_{7-x}$ ($x \approx 1.0$) as an electride, and it is better to represent it as $[Y_2Ti_2O_6]^{2+}(2e^-)$.

Ref. 2 reported the properties of the electride $[Ca_{12}Al_{14}O_{32}]^{2+}(2e^-)$: $[e] \approx 5 \times 10^{19}$ cm^{-3}, $[V_O] \approx 2 \times 10^{21}$ cm^{-3}. The degree of ionization is calculated as $\alpha \approx 1.3\%$. The α value for $[Ca_{12}Al_{14}O_{32}]^{2+}(2e^-)$ is smaller than that of $[Y_2Ti_2O_6]^{2+}(2e^-)$, possibly because $[Ca_{12}Al_{14}O_{32}]^{2+}(2e^-)$ does not have valence variable ions, such as Ti^{4+}.

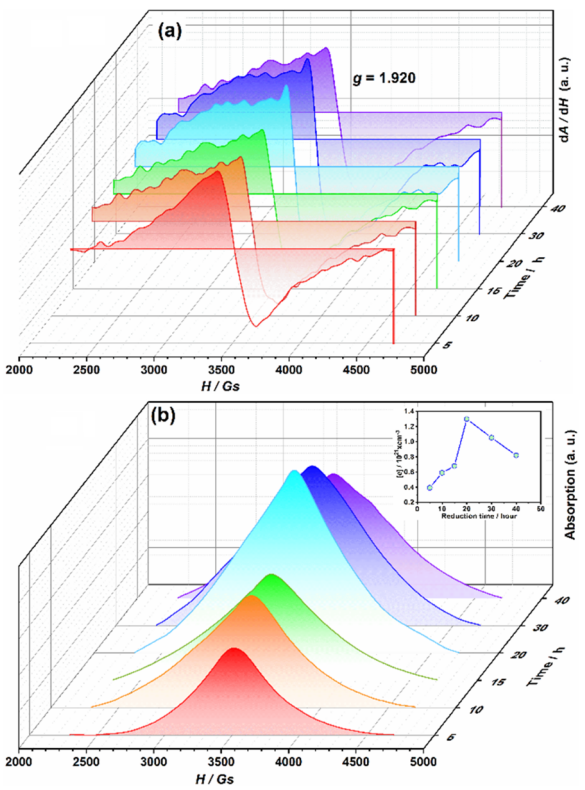

Fig. 7 EPR data of the samples annealed with 0.75 g CaH_2 at 600 °C for various time. (a) Original EPR spectra ("dA/dH–H" plots); (b) absorption peaks to microwave emission (integrations of the dA/dH–H plots); inset in (b): variation of the concentration of unpaired electrons with reduction time.

3.5 DC conductivity measurements

Based on the above discussions, it is known that after annealing with CaH_2 at 600 °C for 20 h, $Y_2Ti_2O_7$ can be reduced to an electride, and its composition can be represented as $[Y_2Ti_2O_6]^{2+}(2e^-)$. Since the electride has loosely bound electrons ($2e^-$), it should have good conductivity. The DC conductivity of the electride was measured in the temperature range 100 K–500 K. Prior to the measurements. The pellet samples were sintered in vacuumed quartz ampoules at 900 °C for 2 h (2.1 section). The data are illustrated in Fig. 8. The electride $[Y_2Ti_2O_6]^{2+}(2e^-)$ has relatively high conductivity, *e.g.* at 300 K, the conductivity $\sigma = 1.09$ S cm^{-1}. In this case, Arrhenius equation ($\sigma = \sigma_0^A e^{-E_a/kT}$, E_a is activation energy, k is Boltzmann constant and σ_0^A is a constant) is not suitable to describe the relationship between the conductivity (σ) and temperature (T). Nevertheless, the variable range hopping molds may be applied to this material. Following Chaudhuri's idea,[21] for the electride $[Y_2Ti_2O_6]^{2+}(2e^-)$, above 230 K, Mott equation is applied to analyze the "$\sigma \sim T$"

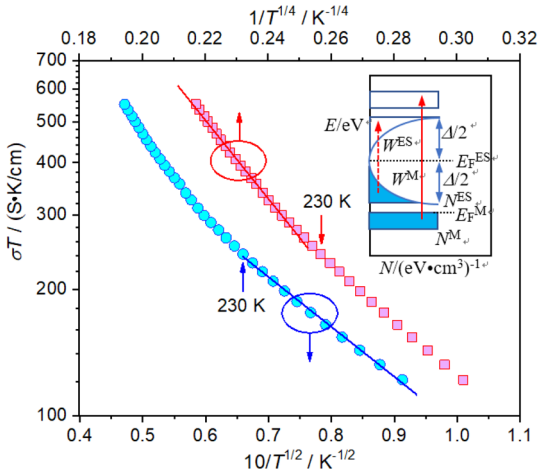

Fig. 8 Variations of conductivity with temperature. Upper: Mott plot (log $T\sigma$–$T^{1/4}$ plot); down: Efros–Shklovskii plot (log $T\sigma$–$T^{1/2}$ plot); inset: schematic diagram of DOS.

data, while below this temperature, Efros–Shklovskii equation is used.

Since $[Y_2Ti_2O_6]^{2+}(2e^-)$ has quite high conductivity and the conductivity does not change very much with temperature, the lattice scattering to the electrons cannot be omitted. The pre-exponential factor in Mott equation should be modified from "σ_0^M" to "σ_0^M/T":

$$\sigma^M = \frac{\sigma_0^M}{T} e^{-\left(\frac{T_0^M}{T}\right)^{1/4}} \quad (10)$$

Here both σ_0^M and $T_O{}^M$ are the constants. The data are represented in the "$\sigma T \sim T^{1/4}$" form (Fig. 8). The line fitting gave the value of 2.054×10^5 K for TOM, by which other parameters for the conductivity were calculated following the equations below:[22]

The density of state (DOS) at Fermi energy N^M is represented as:

$$N^M = N(E_F^M) = \frac{24(\alpha^M)^3}{\pi T_0^M k} \quad (11)$$

a^M is the decade rate of the wave function of the carriers, normally, the value of 2.0 nm^{-1} is given. Furthermore, the hopping distance (R^M) and the hopping energy (W^M) can be calculated as.

$$R^M = \left[\frac{3}{2\pi\alpha^M N(E_F^M) kT}\right]^{1/4} \quad (12)$$

$$W^M = \frac{3}{4\pi(R^M)^3 N(E_F^M)} \quad (13)$$

The calculated results ($T = 400$ K) are listed in Table 1.

As the same reason, the pre-exponential factor of Efros–Shklovskii eqution is also modified as "σ_0^{ES}/T":

$$\sigma = \frac{\sigma_0^{ES}}{T} e^{-\left(\frac{T_0^{ES}}{T}\right)^{1/2}} \quad (14)$$

Here σ_0^{ES} and T_0^{ES} are also the constants. By line fitting, the value of T_0^{ES} was obtained as 717 K, and then, other parameters for the conductivity were calculated according to the following equations:

The Coulomb gap Δ is calculated as:

$$\Delta = \frac{k}{2}(T_0^{ES} T^*)^{1/2} \quad (15)$$

Here, T^* is the temperature maximum that eqn (14) works. For the electride $[Y_2Ti_2O_6]^{2+}(2e^-)$, $T^* = 230$ K. DOS at the energy $E_F^{ES} - \Delta/2$, N^{ES} can be calculated as:

$$N^{ES} = N(E_F^{ES} - \Delta/2) = \frac{3^8\pi^2 k^2 \varepsilon_r^3 \varepsilon_0^3}{2^9 e^6}(T_0^{ES} T^*) \quad (16)$$

Here, ε_r is the relative permittivity of $Y_2Ti_2O_7$, ref. 23 gave the value of 54; ε_0 is the free space permittivity; e is the electron charge. The hopping distance (R^{ES}) can be calculated as:

$$R^{ES} = \frac{1}{4\alpha^{ES}}\left[\frac{T_0^{ES}}{T}\right]^{1/2} \quad (17)$$

Here, α^{ES} is the tunneling exponent, it can be calculated by:

$$\alpha^{ES} = kT_0^{ES}\frac{(\pi N_2)^{1/3}}{10.5} \quad (18)$$

The value of N_2 is given as

$$N_2 = \frac{3^8\pi^2\varepsilon_r^3\varepsilon_0^3}{2^5 e^6} \quad (19)$$

The hopping energy is given as:

$$W = \frac{k}{2}(T_0^{ES} T)^{1/2} \quad (20)$$

The calculated results are listed in Table 1 ($T = 200$ K).

Mott's theory and Efros–Shklovskii's theory are based on different DOS (density of state) features, which are schematically illustrated in the inset in Fig. 8. In Efros–Shklovskii's theory, the DOS varies as parabolic function near Fermi level, which is applied in low temperature range. At higher temperature range, DOS has flat or constant feature by Mott's theory. The parameters listed in Table 1 are basically reasonable. Hopping energy W^M is larger than W^{ES}; both W^M and W^{ES} are larger than the related kT. The hopping distance R^M is shorter than R^{ES}, but both of them are about 1.2 nm. According to the

Table 1 The conduction parameters calculated according to Mott equations and Efros–Shklovskii equations

E–S eqn	T_0^{ES}/K	α^{ES}/nm^{-1}	N^{ES}/$(eV\ cm^3)^{-1}$	R^{ES}/nm	W^{ES}/meV	Δ/meV	T/K	kT meV^{-1}
	7.16×10^2	0.33	4.10×10^{21}	1.35	16	18	200	17

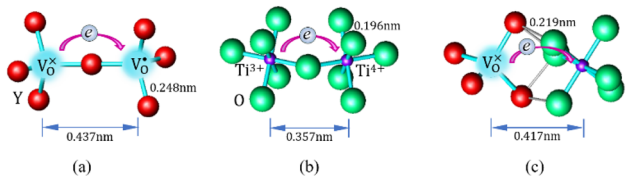

Fig. 9 Schematic diagrams for three possible conduction channels for electrons: (a) $V_O^{\times} \rightarrow V_O^{\cdot}$ through O–Y framework; (b) $Ti^{3+} \rightarrow Ti^{4+}$ through Ti–O framework; (c) $V_O^{\times} \rightarrow Ti^{4+}$ cross two frameworks.

structure of Y_2TiO_7, the electrons in the electride $[Y_2Ti_2O_6]^{2+}(2e^-)$ have three possible transporting channels (Fig. 9): (i) $V_O^{\times} \rightarrow V_O^{\cdot}$ through $[O_2Y_4]$ framework; (ii) $Ti^{3+} \rightarrow Ti^{4+}$ through $[Ti_4O_{12}]$ framework; (iii) $V_O^{\times} \rightarrow Ti^{4+}$ cross two frameworks. In all three channels, the distances (d) for the electron transportation are all about 0.4 nm, which are the minimum distances. R^M and R^{ES} are ~3 times d. Thus, the values of R^M and R^{ES} are in a reasonable scale.

The conductivity of $[Y_2Ti_2O_6]^{2+}(2e^-)$ was also reported by Hayward,[11] $\sigma = 10^{-4}$ S cm^{-1} (295 K). In Hayward's work, conductivity measurements were carried out on pressed powders. Due to poor connection among the grains, the conductivity was low. In this work, sintered pellets were used. Since the connections among the grains were improved, the conductivity was increased significantly ($\sigma = 1.09$ S cm^{-1}). However, the relative densities of the sintered pellets in this work were about 75%. If denser pellets could be obtained, the conductivity may be further improved.

4 Conclusions

The O-depleched pyrochlore samples $Y_2Ti_2O_{7-x}$ were prepared by the solid reducing method. The x value representing the content of V_O was determined by TG analyses. In a proper reductive condition, the sample with $x = 1.0$ was obtained, which is considered as an electride. The composition of the electride is represented as $[Y_2Ti_2O_6]^{2+}(2e^-)$. Here $(2e^-)$ are two loosely trapped electrons in $V_O^{\times}$, which may be ionized, resulting in the production of unpaired electrons. Quantitative analysis of EPR data gave the concentration of unpaired electrons as 1.3×10^{21} cm^{-3}. Since the concentration of loosely bound electrons in electride is quite high, its performance satisfied conductivity (1.09 S cm^{-1} at 300 K). In the preparation process, the samples underwent water-washing and oven-drying. Thus, the electride $[Y_2Ti_2O_6]^{2+}(2e^-)$ obtained in this work is stable in moisture and oven temperatures (*i.e.* below 150 °C).

Although electrides were found quite early, inorganic solid electrides were found quite recently (2003). Due to their special crystal structure and electronic structure, these kinds of materials may have unique properties on electronics, magnetics, and catalysis. However, only a few inorganic solid electrides were reported. It is imperative to search for more novel electrides.

Conflicts of interest

There are no conflicts to declare.

Acknowledgements

We are thankful for financial support from National Natural Science Foundations of China (21371015 and 22271180). Thanks are also given to Ms Yufeng Guo and Mr Jinlong Wang at School of Environment in Tsinghua University for EPR measurements.

Notes and references

1 P. Atkins, T. Overton, J. Rourke, M. Weller, F. Armstrong and M. Hagerman, *Inorganic Chemistry*, 5th edn, W. H. Freeman and Company, New York, 2010, vol. 130, p. 306.
2 S. Matsuishi, Y. Toda, M. Miyakawa, K. Hayashi, T. Kamiya, M. Hirano, I. Tanaka and H. Hosono, *Science*, 2003, **301**, 626.
3 J. Huang, L. Valenzano and G. Sant, *Chem. Mater.*, 2015, **27**, 4731.
4 Y. Toda, S. Matuishi, K. Hayashi, K. Ueda, T. Kamiya, M. Hirano and H. Hosono, *Adv. Mater.*, 2004, **16**, 685.
5 Y. Inoue, M. Kitano, S.-W. Kim, T. Yokoyama, M. Hara and H. Hosono, *ACS Catal.*, 2014, **4**, 674.
6 J. Sharif, M. Kitano, Y. Inoue, Y. Niwa, H. Abe, T. Yokoyama, M. Hara and H. Hosono, *J. Phys. Chem. C*, 2015, **119**, 11725.
7 N.-H. Chan, R. K. Sharma and D. M. Smyth, *J. Am. Ceram. Soc.*, 1981, **64**, 556.
8 X. Kuang, X. Jing and Z. Tang, *J. Am. Ceram. Soc.*, 2006, **89**, 241.
9 J. M. Longo, P. M. Raccah and J. B. Goodenough, *Mater. Res. Bull.*, 1969, **4**, 191.
10 G. Sala, M. J. Gutmann, D. Prabhakaran, D. Pomaranski, C. Mitchelitis, J. B. Kycia, D. G. Porter, C. Castelnovo and J. P. Goff, *Nat. Mater.*, 2014, **13**, 488.
11 M. A. Hayward, *Chem. Mater.*, 2005, **17**, 670.
12 J. A. Weil, J. R. Bolton and J. E. Wertz, *Electron Paramagnetic Resonance*. John Wiley & Sons, Inc. New York, 1994, p. 496.
13 F. Matteucci, G. Cruciani, M. Dondi, G. Baldi and A. Barzanti, *Acta Mater.*, 2007, **55**, 2229.
14 M. A. Subramanian, G. Aravamudan and G. V. Subba Rao, *Prog. Solid State Chem.*, 1983, **15**, 55.
15 W. W. Barker, P. S. White and O. Knop, *Can. J. Chem.*, 1976, **54**, 2316.
16 A. W. Sleight, *Mater. Res. Bull.*, 1971, **6**, 775.
17 S. K. Misra, S. I. Andronenko, D. Tipikin, J. H. Freed, V. Somani and O. Prakash, *J. Magn. Magn. Mater.*, 2016, **401**, 495.
18 M. Ivanovskaya, K. Chernyakova, E. Ovodok, S. Poznyak, D. Kotsikau and I. Azarko, *Mater. Chem. Phys.*, 2022, **278**, 125703.
19 D. Zhang, X. Ma, H. Zhang, Y. Liao and Q. Xiang, *Mater. Today Energy*, 2018, **10**, 132.
20 K. Xie, N. Umezawa, N. Zhang, P. Reunchan, Y. Zhang and J. Ye, *Energy Environ. Sci.*, 2011, **4**, 4211.
21 A. Ganguly, S. K. Mandal, S. Chaudhuri and A. K. Pal, *J. Appl. Phys.*, 2001, **90**, 5652.
22 M. H. Sage, G. R. Blake and T. T. M. Palstra, *Phys. Rev.*, 2008, **B77**, 155121.
23 T.-T. Tao, L.-X. Wang and Q.-T. Zhang, *J. Alloy. Compd*, 2009, **486**, 606.